

Measurement of jet cross sections in ATLAS

J. Poveda on behalf of the ATLAS Collaboration

University of Wisconsin-Madison, 1150 University Avenue, Madison, WI 53706-1390, USA

Abstract. Jet cross sections have been measured in proton-proton collisions at a centre-of-mass energy of 7 TeV using the ATLAS detector at the Large Hadron Collider. The anti- k_r algorithm is used to identify jets. Inclusive single-jet differential cross sections are presented as functions of jet transverse momentum and rapidity. Dijet cross sections are presented as functions of dijet mass and angle. The measurements extend the previously measured kinematic region to higher rapidities, and to both higher and lower values of transverse momentum. The results are compared to next-to-leading-order QCD calculations matched to leading-logarithmic parton showers.

Keywords: CERN, LHC, ATLAS, inclusive jet p_T , dijet mass, QCD

PACS: 13.87.-a, 12.38.Qk

INTRODUCTION

Jet cross section measurements are one of the main observables in high-energy particle physics, and at the Large Hadron Collider (LHC) they can test quantum chromodynamics (QCD) in a new kinematic regime and can be used to tune descriptions of parton distribution functions (PDFs), Monte Carlo generators, etc.

First ATLAS results on jet production cross sections using 17 nb^{-1} were reported in summer 2010 [1]. These proceedings report on the inclusive jet and dijet cross section measurements in ATLAS using the full 2010 data sample of 37.3 pb^{-1} [2].

The ATLAS detector is described in detail in [3]. The calorimetry comprises several systems which provide a total coverage of $|\eta| < 4.9$. The electromagnetic calorimetry is provided by high granularity liquid argon calorimeters (LAr) that are divided into barrel ($|\eta| < 1.475$) and end-cap ($1.375 < |\eta| < 3.2$) regions. The hadronic calorimeter is assembled in three distinct regions: the barrel ($|\eta| < 0.8$) and the extended barrel ($0.8 < |\eta| < 1.7$), both being scintillator/steel calorimeters; the Hadronic End-Cap (HEC; $1.5 < |\eta| < 3.2$) using LAr/Cu calorimeter modules; and finally the Forward Calorimeter (FCal; $3.1 < |\eta| < 4.9$) instrumented with LAr/Cu and LAr/W modules to provide electromagnetic and hadronic energy measurements respectively.

ANALYSIS DESCRIPTION

Definition of Observables

Inclusive single-jet double-differential cross sections are measured as a function of jet p_T and y in the region $p_T > 20 \text{ GeV}$, $|y| < 4.4$, where the rapidity $y = \frac{1}{2} \ln \frac{E+p_z}{E-p_z}$ is used instead of η for jets and massive particles. Dijet double-differential cross sections are

measured as a function of the dijet mass, m_{12} , binned in the maximum rapidity of the two leading jets, $|y|_{\max} = \max(|y_1|, |y_2|)$.

Cross sections results are compared to next-to-leading order (NLO) perturbative QCD (pQCD) predictions corrected for non-perturbative effects, where the theoretical uncertainties from scale variations, parton distribution functions, and non-perturbative corrections have been accounted for.

Data and Event Selection

In this analysis jets are identified using the anti- k_t jet algorithm [4]. The value used for the clustering parameter R can be seen intuitively as the radius of a cone jet in the plane (ϕ, y) of azimuthal angle and rapidity. Jets are corrected for calorimeter non-compensation, upstream material and other effects using calibration factors obtained from Monte Carlo and validated with test-beam and collision-data studies [5, 6].

The inclusive jet cross section is computed for jets with $p_T > 20$ GeV and $|y| < 4.4$. In addition, for the dijet mass measurements, events are selected in which the leading jet has $p_T > 30$ GeV and $|y| < 4.4$, and at least one sub-leading jet has $p_T > 20$ GeV and $|y| < 4.4$. Events are discarded if they contain any jet failing basic quality selection criteria that reject detector noise and non-collision backgrounds [7].

Three different triggers have been used in this measurement: the Minimum Bias Trigger Scintillators (MBTS); the central jet trigger, covering $|\eta| < 3.2$; and the forward jet trigger, spanning $3.1 < |\eta| < 4.9$. For each p_T -bin considered in this analysis, a fully efficient ($> 99\%$) trigger with the smallest possible prescale factor is used.

Data Correction and Systematic Uncertainties

All corrections for detector inefficiencies and resolutions are performed in a single step using a bin-by-bin correction derived from the Pythia [8] Monte Carlo simulation. Then for each measured distribution, the ratio between the final-state particle-level cross section and the equivalent distribution after detector simulation and reconstruction is applied as a correction factor to the measured data.

The largest systematic uncertainty affecting this analysis arises from the jet energy scale varying between 10-50% in the kinematic range studied. The detector unfolding uncertainties (which include jet energy resolution, angular resolution, cross section shape, etc.) are approximately 5-10% over most of the kinematic range studied. The luminosity uncertainty has recently been reduced to only 3% [9] and various other sources of systematic uncertainties such as trigger or jet reconstruction efficiency were found to have a small impact on the results (1-2%).

RESULTS

Figure 1 shows the inclusive jet and dijet cross sections compared with the NLO pQCD prediction for $R = 0.6$ obtained with NLOJET++ 4.1.2 [10]. As shown, data and theory

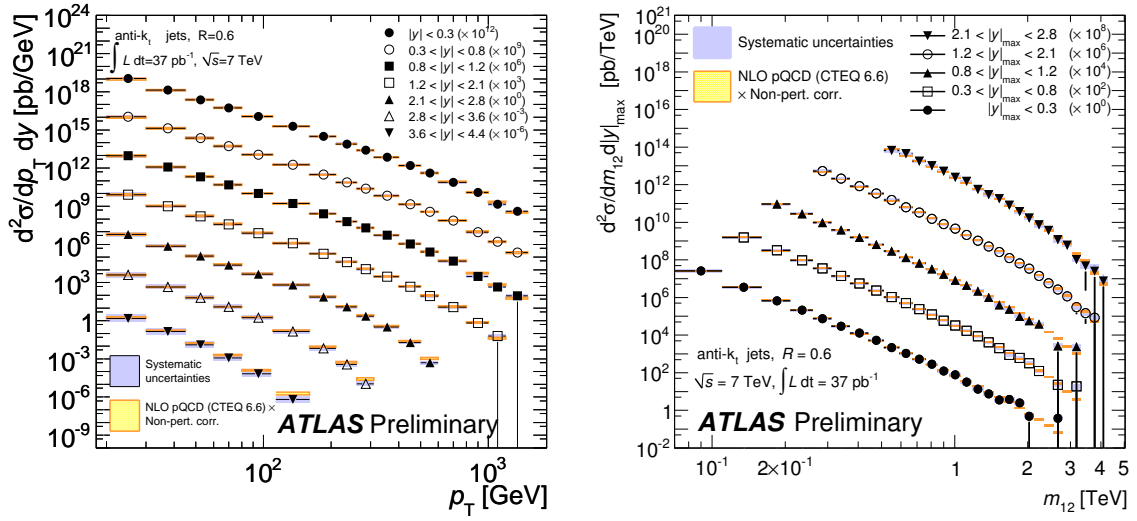


FIGURE 1. On the left, inclusive jet double-differential cross section as a function of jet p_T in different regions of $|y|$. On the right, dijet double-differential cross section as a function of dijet mass, binned in the maximum rapidity of the two leading jets $|y|_{\max}$. Results are shown for jets identified using the anti- k_T algorithm with $R = 0.6$. The data are compared to NLO pQCD calculations to which non-perturbative corrections have been applied. For convenience, the cross sections are multiplied by the factors indicated in the legends.

are in good agreement over several orders of magnitude in cross section although some differences are observed at high jet p_T and $|y|$.

The ratio of the measured inclusive jet cross sections over the theoretical predictions from NLO pQCD obtained with different PDF sets is shown in Figure 2. Agreement with data is observed in all the cases, although at high p_T and $|y|$ data are below the theoretical prediction. In this region, CTEQ 6.6 [11] is disfavoured and MSTW 2008 [12], NNPDF 2.1 [13, 14], and HERAPDF 1.5 [15] tend to agree better with data. Comparisons with parton shower Monte Carlos with NLO matrix elements are shown in [2] where data are above the Monte Carlo prediction. Results for $R = 0.4$ can also be found in [2].

SUMMARY

Cross section measurements have been presented for inclusive jet production as a function of jet transverse momentum, and for dijet production as a function of the invariant mass of the two leading jets. These are based on the full data sample collected with the ATLAS detector during 2010, which corresponds to $37.3 \pm 1.2 \text{ pb}^{-1}$ of integrated luminosity. Results have been compared to fixed order NLO pQCD calculations corrected for non-perturbative effects with an overall good agreement, although the cross sections predicted by theory are larger than those measured at large transverse momenta and dijet mass.

These results constitute a validation of QCD in a new kinematic regime and are sensitive to PDFs in regions currently poorly constrained.

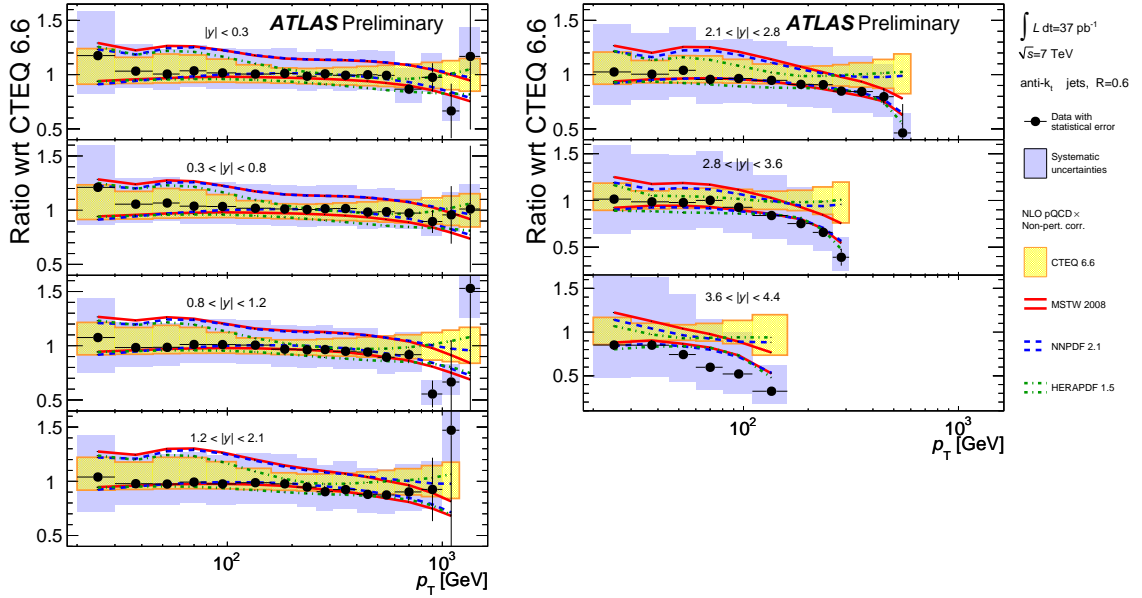


FIGURE 2. Ratio of the data to the theoretical prediction for the inclusive jet double-differential cross section as a function of jet p_T in different central regions of $|y|$ for jets identified using the anti- k_t algorithm with $R = 0.6$. The theoretical error bands obtained by using different PDF sets (CTEQ 6.6, MSTW 2008, NNPDF 2.1, HERAPDF 1.5) are shown. The data points and the error bands are normalized to the theoretical predictions obtained by using the CTEQ 6.6 PDF.

REFERENCES

1. G. Aad, et al., *Eur.Phys.J.* **C71**, 1512 (2011), 1009.5908.
2. ATLAS Collaboration, ATLAS-CONF-2011-047 (2011), URL <http://cdsweb.cern.ch/record/1338578/files/ATLAS-CONF-2011-047.pdf>.
3. G. Aad, et al., *JINST* **3**, S08003 (2008).
4. M. Cacciari, G. Salam, and G. Soyez, *JHEP* **0804**, 063 (2008), arXiv:0802.1189.
5. ATLAS Collaboration, ATLAS-CONF-2010-050 (2010), URL <http://cdsweb.cern.ch/record/1281305/files/ATLAS-CONF-2010-050.pdf>.
6. E. Abat, et al., *Nucl.Instrum.Meth.* **A621**, 134–150 (2010).
7. ATLAS Collaboration, ATLAS-CONF-2010-038 (2010), URL <http://cdsweb.cern.ch/record/1277678/files/ATLAS-CONF-2010-038.pdf>.
8. T. Sjostrand, S. Mrenna, and P. Skands, *JHEP* **05**, 026 (2006), hep-ph/0603175.
9. ATLAS Collaboration, ATLAS-CONF-2010-060 (2010), URL <http://cdsweb.cern.ch/record/1281333/files/ATLAS-CONF-2010-060.pdf>.
10. Z. Nagy, *Phys. Rev.* **D68**, 094002 (2003), hep-ph/0307268.
11. J. Pumplin, et al., *JHEP* **07**, 012 (2002), hep-ph/0201195.
12. A. D. Martin, W. J. Stirling, R. S. Thorne, and G. Watt, *Eur. Phys. J.* **C63**, 189–285 (2009), 0901.0002.
13. R. D. Ball, et al., *Nucl. Phys.* **B838**, 136–206 (2010), arXiv:1002.4407.
14. S. Forte, E. Laenen, P. Nason, and J. Rojo, *Nucl. Phys.* **B834**, 116–162 (2010), arXiv:1001.2312.
15. H1 and ZEUS Collaborations, HERAPDF 1.5 (preliminary), H1prelim-10-142, ZEUS-prel-10-018 (2010), URL https://www.desy.de/hlzeus/combined_results/index.php?do=proton_structure.